

A Linear Paul Trap without the use of the Transverse Quadrupole Field

Kunihiro KOJIMA, Masato GOTO, Hiroyuki HIGAKI, Kiyokazu ITO and Hiromi OKAMOTO

*Graduate School of Advanced Science and Engineering, Hiroshima University,
1-3-1 Kagamiyama, Higashi-Hiroshima 739-8530, Japan*

(Received 7 November 2021 / Accepted 12 December 2021)

A detailed experimental study has been conducted to demonstrate the efficient confinement of ions in the popular four-rod configuration of a linear Paul trap without exciting the transverse radio-frequency (rf) quadrupole field. The three-dimensional (3D) ion confinement is achieved with an identical rf voltage applied to the end electrodes. The optimum operating region is visualized in the stability *tune* diagram, which indicates that a large number of ions can be stored by adjusting a few fundamental parameters. The lifetime of an ion cloud in the present linear trap is over a second (corresponding to a million rf cycles), long enough for various practical applications. It is also shown through 3D numerical simulations that one can easily extract ions from the trap at a low loss rate below 10%.

© 2022 The Japan Society of Plasma Science and Nuclear Fusion Research

Keywords: non-neutral plasma, linear Paul trap, radio-frequency confinement of ion, stability diagram

DOI: 10.1585/pfr.17.1406003

1. Introduction

A variety of charged-particle trapping systems have been developed so far and employed for diverse purposes including mass spectrometry [1–4], quantum computing [5–9], anti-matter production [10–14], beam physics [15–18], the establishment of time and frequency standards [19–23], etc. Among them, the so-called “Paul trap” is likely the most popular device that rely on electric fields for particle confinement [24]. Since three-dimensional (3D) confinement of a charged-particle cloud at rest is not feasible with a static electric potential only, a Paul trap makes use of a radio-frequency (rf) field.

In a standard linear Paul trap (LPT), four cylindrical rods are arranged symmetrically around the trap axis as illustrated in Fig. 1. Proper rf voltages are applied to the rods to create an alternating gradient quadrupole field in the transverse x - y plane perpendicular to the z -direction. The scalar potential for transverse ion focusing is given by

$$\phi_{\perp} \approx \frac{V_Q(t)}{r_0^2}(x^2 - y^2), \quad (1)$$

where $V_Q(t)$ is the rf quadrupole voltages added to all three sections in Fig. 1, and r_0 is the minimum distance from the z -axis to the electrode surface. The axial confinement potential ϕ_{\parallel} is usually provided by DC bias voltages added to the two end sections (END-A and END-B) electrically isolated from the central section (ES) where ions are accumulated; these static biases make potential barriers on both sides of the ES to prevent ions from escaping axially. The total electric potential employed for 3D ion confinement in a regular LPT is thus the sum of ϕ_{\perp} and ϕ_{\parallel} .

author's e-mail: okamoto@sci.hiroshima-u.ac.jp

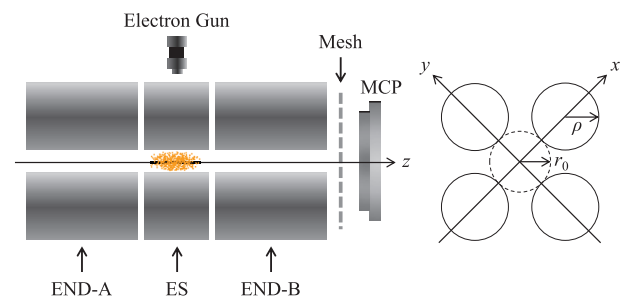


Fig. 1 A schematic of the 3D ion trap used for the present experiment. The trap is divided into three electrically isolated sections referred to as “ES (Experiment Section)”, “END-A”, and “END-B”. Ions are confined in the ES above which an electron gun is placed to ionize neutral gas atoms. A metallic mesh is inserted between the trap and a micro-channel plate (MCP) detector to reduce the switching noise from the end electrodes and to minimize the aperture-field distortion caused by the high DC voltage (−1.35 kV) on the MCP surface. The radii of the aperture and electrode rods are $r_0 = 5$ mm and $\rho = 5.75$ mm, respectively. The central electrodes for the ES are 8.9 mm long, which makes the axial potential well nearly parabolic around the trap center. The axial length of the two end sections is 30 mm.

The on-axis configuration of the potential well formed by the DC biases depends on the mechanical design of the trap. It will be more like a square-well shape when the ES is considerably long compared to the aperture size (because the central electrodes shield the DC potentials on the end sections). The potential well can be made near-parabolic with the ES electrodes comparable in length to

the aperture size $2r_0$.

Provided that the overall dimension of the trap structure is much smaller than the rf wavelength, which is typically the case with most ion traps, the electric potential within the aperture approximately satisfies Laplace equation. The focusing effect along the axial z -direction is then accompanied inevitably by the corresponding defocusing effect in the transverse x - y plane. When $r_0 = 5$ mm and $\rho = 5.75$ mm in Fig. 1, the optimum length of the ES that makes the quadratic terms in ϕ_{\parallel} most dominant is 8.9 mm [25]. Assuming that all eight electrode rods in the END-A and END-B sections have an identical voltage V_{END} , we can write an approximate solution of Laplace equation as

$$\phi_{\parallel} \approx \frac{V_{\text{END}}}{\ell_z^2} \left(z^2 - \frac{x^2 + y^2}{2} \right), \quad (2)$$

where ℓ_z is the characteristic length determined by the electrode design, and the origin of the coordinate system is chosen at the trap center. Under the boundary condition of the trap geometry in Fig. 1, we find $\ell_z \approx 8.23$ mm [25]. V_{END} is generally set constant in regular LPTs as mentioned above. Note that the transverse electric force produced by ϕ_{\parallel} is not quadrupolar but axisymmetric.

An important point indicated by Eq. (2) is that the DC bias introduced originally for axial ion confinement yields the transverse quadratic terms as well. Whether these terms work as focusing or defocusing depends on the sign of the bias voltage V_{END} . If V_{END} is not static but periodically changes its sign, we may be able to accomplish simultaneous ion confinement in all three dimensions without exciting the quadrupole rods in the ES. A similar idea was previously discussed in Ref. [26] though no detailed experimental study of confined ion stability has been done yet with a linear structure of the four-rod configuration.

In the following, we demonstrate that not static but time-varying rf voltages on the end sections actually suffice to confine a large number of ions three-dimensionally; it is unnecessary to provide an additional time-varying potential ϕ_{\perp} for transverse ion confinement. A regular LPT sketched in Fig. 1 is converted to the proposed 3D harmonic trap, though a much simpler structure is acceptable as we no longer need the transverse quadrupole field. For instance, the harmonic component in Eq. (2) can be generated even if all three quadrupole sections in Fig. 1 are replaced by cylindrical electrodes. The four-rod configuration considered here is, however, practically convenient for ion production and observation because of a wide opening between the electrodes, which provides easy access to the ion confinement region from outside. As shown later, it is also possible to extract ions very easily at high transmission efficiency.

The paper is organized as follows. In Sec. 2, we introduce the concept of ‘‘tune’’ commonly employed in beam physics [27, 28]. We then move on to experimental results and related numerical simulation data in Sec. 3. After showing a typical signal from the MCP detector, the opti-

um operating condition is revealed in the tune space. The lifetime of an ion cloud stored in the present LPT is also measured. A short summary is finally given in Sec. 4.

2. Tune of the Ion Oscillation

Let us assume that both end sections have an identical rf voltage of the form

$$V_{\text{END}}(t) = U - V_{\text{rf}} \sin \omega t, \quad (3)$$

where V_{rf} is the constant amplitude of the rf voltage oscillating at the angular frequency ω , and U is the DC bias. The motion of an ion under the influence of the linear potential in Eq. (2) then obeys the Mathieu equations

$$\frac{d^2 x}{d\tau^2} - (a - 2q \cos 2\tau)x = 0, \quad (4)$$

$$\frac{d^2 z}{d\tau^2} + 2(a - 2q \cos 2\tau)z = 0, \quad (5)$$

where a and q are the Mathieu parameters defined by $a = 4eU/m\ell_z^2\omega^2$, $q = 2eV_{\text{rf}}/m\ell_z^2\omega^2$ with e and m being the charge state and mass of the confined ion, and $\tau = \omega t/2$. The equation of ion motion in the y direction is the same as Eq. (4). It is well-known that the solution of either equation above becomes unstable due to parametric resonance, depending on the values of a and q [24].

We here use the transverse and axial tunes, rather than the Mathieu parameters, to describe the stability of the ion motion. The tune is directly linked to the characteristic exponent of the solution of the Mathieu equation. It is equal to the number of the secular oscillation per rf period and ranges from 0 to 0.5 in the first Mathieu stability domain. We denote the tunes in the three spatial degrees of freedom to be (ν_x, ν_y, ν_z) . They can readily be calculated from the envelope function η_w satisfying

$$\frac{d^2 \eta_w}{d\tau^2} + K_w(\tau)\eta_w - \frac{1}{\eta_w^3} = 0, \quad (6)$$

where the subscript w stands for either x or y or z . For the ion oscillation described by Eqs. (4) and (5), $K_z(\tau) = 2(a - 2q \cos 2\tau)$ and $K_w(\tau) = -a + 2q \cos 2\tau$ for $w = x$ and y . The tune is evaluated by substituting the stationary solution of Eq. (6) into

$$\nu_w = \frac{1}{2\pi} \int_{\tau}^{\tau+\pi} \frac{1}{\eta_w^2} d\tau. \quad (7)$$

In the present case, the two transverse tunes are always equal, namely, $\nu_x = \nu_y (\equiv \nu_{\perp})$ because the focusing force in the x - y plane is axisymmetric.

3. Results

3.1 Experiment setup

The ion species adopted for this experimental study is $^{40}\text{Ar}^+$ that can readily be produced from neutral Ar gas atoms through electron bombardment. The kinetic energy

of electrons from the e -gun was chosen to be about 100 eV. The base pressure in the vacuum chamber is 4×10^{-8} Pa, which is worsened by roughly two orders of magnitudes during the ionization process that lasts for 1 s. The initial ion number can be controlled by changing the electron-beam current and Ar-gas pressure. After a sufficient number of ions are accumulated in the ES, we shut down the electron beam and then start to test the trap performance.

The operating rf frequency was fixed at $\omega/2\pi = 1$ MHz. The maximum rf amplitude, $\max(V_{\text{rf}})$ in Eq. (3), necessary to cover the whole first stability region of the Mathieu equation is then 360 V. The rf voltage available with our current power supply system is, however, less than 140 V, so we gave exactly the same rf voltage $V_{\text{ES}}(t)$ to all four rods in the ES. $V_{\text{ES}}(t)$ is out of phase with $V_{\text{END}}(t)$ by 180 degrees (see Fig. 2 (b)). This rf bias allows us to explore the dynamic effect physically equivalent to the simple case where the ES is grounded while the electrodes in both end sections have the rf voltage of the magnitude

$$V_{\text{END}}(t) - V_{\text{ES}}(t).$$

3.2 Ion transport to the MCP detector

The experimental data in Fig. 2 is a piece of indisputable evidence that the proposed ion trapping scheme works fine. The upper panel exhibits an example of the MCP output when the operating tunes are fixed at $(\nu_{\perp}, \nu_z) = (0.12, 0.12)$. The corresponding rf voltages applied to the three sections (ES, END-A and END-B) are shown in the middle panel. The ion extraction procedure is initiated at $t = 0$. The rf amplitude V_{rf} is maintained throughout the extraction process to minimize ion losses in the ES after $t = 0$. The absolute value of the extraction bias U_{ext} on the end sections, set at zero before $t = 0$, gradually increases to a certain value in a few μs . Needless to say, the bias must be positive (negative) on the END-A (END-B) to eject positively charged ions toward the MCP detector. In the case of Fig. 2 (b), U_{ext} has finally reached 50 V at $t \approx 5 \mu\text{s}$. This finite rise time is determined by the characteristics of the rf circuit.

It turns out from Fig. 2 (c) that the number of Ar^+ ions confineable in our trap is of the order of 10^5 at least. The experimental data also indicates that U_{ext} must be sufficiently high to maximize the ion transmission efficiency. In fact, the transverse focusing force is lost once ions come into the END-B section of 30 mm long. We, therefore, need to accelerate all ions axially such that they reach the MCP before hitting an electrode.

Particle tracking simulations were performed to figure out how much percentage of ions can reach the MCP. We developed a 3D simulation code in which the effect of arbitrary external electric fields can be taken into account. The exact scalar potential under the boundary condition of the trap geometry depicted in Fig. 1 was first calculated with a 3D Maxwell equation solver and then incorporated in the code. Figure 3 shows a typical result when $(\nu_{\perp}, \nu_z) = (0.12, 0.12)$. The initial distribution assumed here is the Gaussian type whose root-mean-squared size is about 1.1 mm in all three spatial directions. At $t = 0$, the bias voltage on the END-B begins to decrease linearly to -50 V in 5 μs . About 94% of ions stored in the ES are successfully transported to the MCP in this example. We carried out 2500 independent simulations changing the operating tunes within the range $0.05 \leq \nu_{\perp}, \nu_z \leq 0.3$ and confirmed that the transmission efficiency is better than 92.5% at the initial ion-cloud temperature of 0.3 eV when $U_{\text{ext}} = 50$ V. The transmission certainly becomes higher at lower temperature. According to the data in Fig. 2 (c), a similar transmission efficiency is expected as long as the extraction bias U_{ext} exceeds around 10 V.

3.3 Stability map

The number of Ar^+ ions surviving after the storage period of 50 ms (5×10^4 rf cycles) was measured at 1900 different operating points and color-coded in the tune

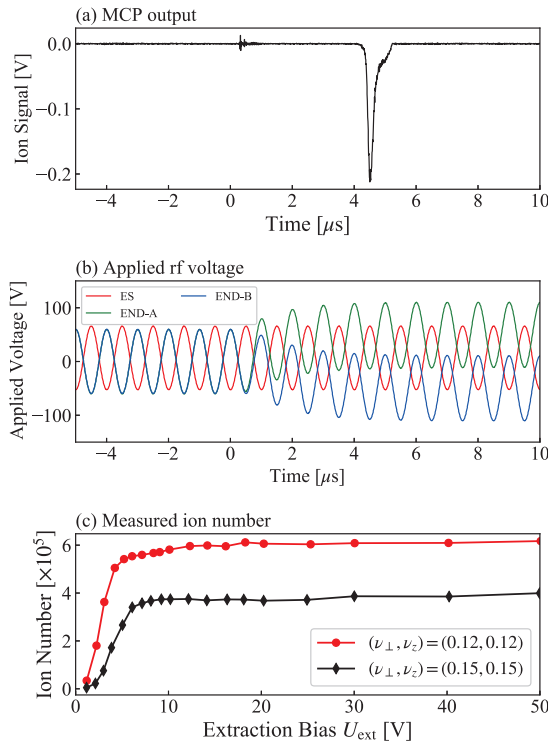


Fig. 2 Experimental results. (a) Example of the ion signal detected with the MCP. (b) Rf voltages applied to the ES (red line), END-A (green line), and END-B (blue line) when $(\nu_{\perp}, \nu_z) = (0.12, 0.12)$. The extraction bias is triggered at $t = 0$ before which the rf voltages on the END-A and END-B have completely overlapped. The bias voltages on the end sections have opposite signs; namely, $+U_{\text{ext}}$ on the END-A and $-U_{\text{ext}}$ on the END-B. (c) Measured ion number vs. extraction bias U_{ext} . The number of ions after the storage period of 50 ms is measured at two different operating points. The ion number plotted here has been calibrated in consideration of the opening ratio of the mesh placed between the trap and MCP.

space. The resultant tune diagram in Fig. 4 clearly indicates that the most preferable operating area lies along the line $\nu_{\perp} - \nu_z = 0$; in other words, the axial and transverse tunes should be equalized for better stability of trapped ions. The number of confineable ions is maximized in the range $0.12 \lesssim \nu_{\perp}, \nu_z \lesssim 0.13$ where 7×10^5 ions or more can survive in the ES for 50 ms. Since the three tunes are about equal, the ion cloud becomes nearly spherical (see Fig. 3 (a)). The maximum ion number achieved in the experiment was 9.1×10^5 at $(\nu_{\perp}, \nu_z) = (0.123, 0.128)$. The optimum operating condition experimentally found here for the LPT without ϕ_{\perp} could apply to the so-called *three-dimensional quadrupole trap* composed of two hyperboloidal end-cap electrodes and a ring electrode of a hyperbolic cross-section because the ion motion in either trap obeys Eqs. (4) and (5) approximately [24].

The stability of an ion cloud is considerably worsened when a low value ($\lesssim 0.1$) is chosen for ν_{\perp} and/or ν_z . This is natural because the operating point is too close to the boundaries of the Mathieu stability region. Note also that

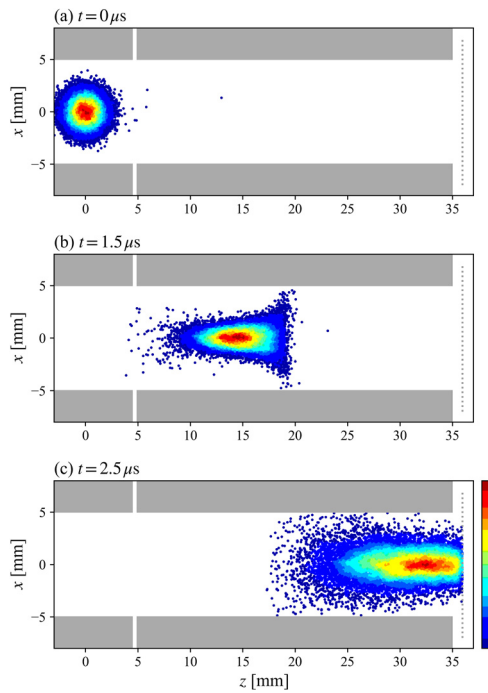


Fig. 3 Particle tracking simulation of ion extraction from the trap. The transverse and axial tunes are adjusted to $(\nu_{\perp}, \nu_z) = (0.12, 0.12)$. The Coulomb interaction among particles is ignored for simplicity. The three panels show the ion distributions observed at three different timings: (a). just before the axial potential barrier on the MCP side is dropped, (b). $1.5 \mu\text{s}$ after ion ejection, and (c). $2.5 \mu\text{s}$ after ion ejection. The Gaussian distribution is assumed initially for all six canonical variables. The initial temperature is set at 0.3 eV, considering past experimental data obtained in a LPT of a similar size [15, 29]. The gray-shaded areas represent the positions of the cylindrical electrodes of the ES and END-B.

the electric potential in the ES is not exactly quadratic as given in Eq. (2) but inevitably includes weak nonlinearities, some of which will be enhanced by mechanical errors unavoidable in reality. We thus expect undesirable nonlinear effects that affect the plasma stability, leading to extra ion losses especially in the vicinity of the stability boundaries.

3.4 Lifetime of confined ions

Additional information important in practice is the lifetime of an ion cloud formed in the trap. Figure 5 shows the time evolution of the surviving ion number $N_{\text{ion}}(t)$ measured at $(\nu_{\perp}, \nu_z) = (0.08, 0.08)$, $(0.09, 0.09)$, and $(0.12, 0.12)$. In this experiment, we somewhat lowered the Argon pressure in the ionization process as it is unnecessary to maximize the number of stored ions. This is why the initial ion number at each operating point in Fig. 5 is a bit smaller than the value achieved in Fig. 4.

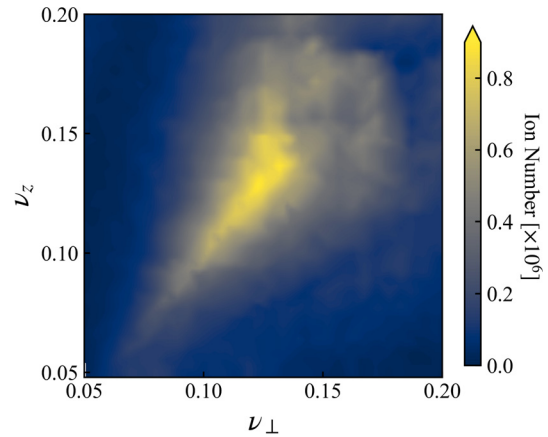


Fig. 4 Tune dependence of the stored ion number measured with the MCP. The ion storage period is fixed at 50 ms.

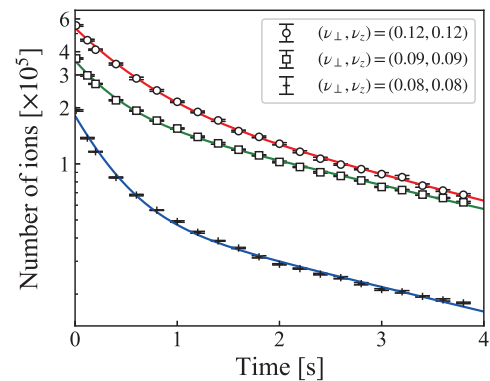


Fig. 5 Number of surviving ions vs. confinement time. We repeated the same measurement procedure five times at the three operating points $(\nu_{\perp}, \nu_z) = (0.08, 0.08)$, $(0.09, 0.09)$, and $(0.12, 0.12)$ and took the average to determine the positions of the markers. The error bars are only as large as the size of each marker. The solid lines are the fitting curves obtained with the exponential function in Eq. (8).

We recognize that there are two distinct regimes of ion decay. Similar ion-decay behavior has been often observed in ordinary LPTs with the rf quadrupole potential ϕ_{\perp} on [30]. All three data in Fig. 5 can be fitted fairly well with a two-component exponential function

$$N_{\text{ion}}(t) = N_S \exp\left(-\frac{t}{T_S}\right) + N_L \exp\left(-\frac{t}{T_L}\right), \quad (8)$$

where N_S , N_L , T_S , and T_L are fitting parameters. The first term on the right-hand side corresponds to the relatively fast decay in the early stage ($t \lesssim 1$ s) while the second term to the slow decay that follows. T_S is estimated to be 510 ms at $(\nu_{\perp}, \nu_z) = (0.12, 0.12)$, longest among the three; it becomes a bit shorter than 400 ms in other two cases. T_L is less sensitive to the operating points. The fitting results are the following: $T_L = 2.93$ s, 3.39 s, and 3.30 s at $(\nu_{\perp}, \nu_z) = (0.12, 0.12)$, (0.09, 0.09), and (0.08, 0.08), respectively.

It should also be informative to compare the present results with those in the regular case where ϕ_{\perp} is switched on for transverse ion confinement. We applied the rf voltages of quadrupole symmetry to all three sections in Fig. 1 while a DC bias potential was added to the two end sections for axial ion confinement. In this common LPT operating mode, we were able to store 3×10^6 Ar⁺ ions for 10 ms at $(\nu_{\perp}, \nu_z) = (0.14, 0.074)$. The optimum ν_z is about half of ν_{\perp} , which makes the ion cloud axially expanded to some degree; namely, the spatial profile of the cloud is ellipsoidal rather than spherical. The estimated decay constants were $T_S = 750$ ms and $T_L = 3.72$ s. The performance of the linear trap is indeed improved by the excitation of the additional rf confinement field in the transverse directions, but these numbers are not very far from what we got with the much simpler ion-trapping scheme studied in this paper.

4. Summary

We examined the performance of a linear ion trap that has the ordinary four-rod structure but employs no transverse quadrupole potential. Theoretically, 3D ion confinement should be achievable by applying an rf voltage only to the end sections; all eight electrode rods in the END-A and END-B sections in Fig. 1 are excited by the same rf voltage while the four rods in the ES may be simply grounded or equally biased. This simplified ion-trapping scheme was tested through experiment and supporting numerical simulations. In the present study, the performance limitation of our power supply system forced us to add an identical rf bias to all four electrode rods in the ES (see Fig. 2 (b)).

We confirmed that a large number of ions can be stored for a long period when the operating point is properly chosen in the tune diagram. The trapped ion cloud is most stable when the three tunes are adjusted to 0.12 or

slightly higher. More than 10^5 ions can then be confined for a few seconds corresponding to a few million rf cycles. It is possible to extract stored ions from the trap at a loss rate below 10% by quickly biasing the electrodes in the end sections with the rf potential kept on.

- [1] W. Paul, *Rev. Mod. Phys.* **62**, 531 (1990).
- [2] S. Maher, F.P.M. Jjunju and S. Talor, *Rev. Mod. Phys.* **87**, 113 (2015).
- [3] J. Dilling, K. Blaum, M. Brodeur and S. Eliseev, *Annu. Rev. Nucl. Part. Sci.* **68**, 45 (2018).
- [4] H.B. Pedersen, D. Strasser, S. Ring *et al.*, *Phys. Rev. Lett.* **87**, 055001 (2001).
- [5] J.I. Cirac and P. Zoller, *Phys. Rev. Lett.* **74**, 4091 (1995).
- [6] R. Blatt and D. Wineland, *Nature* **453**, 1008 (2008).
- [7] P. Schindler, D. Nigg, T. Monz *et al.*, *New J. Phys.* **15**, 123012 (2013).
- [8] C.D. Bruzewicz, J. Chiaverini, R. McConnell *et al.*, *Appl. Phys. Rev.* **6**, 021314 (2019).
- [9] C. Monroe, W.C. Campbell, L.-M. Duan *et al.*, *Rev. Mod. Phys.* **93**, 025001 (2021).
- [10] M. Amoretti, C. Amsler and G. Bonomi, *Nature* **419**, 456 (2002).
- [11] C.M. Surko and R.G. Greaves, *Phys. Plasmas* **11**, 2333 (2004).
- [12] G.B. Andersen, M.D. Ashkezari, M. Baquero-Ruiz *et al.*, *Nature* **468**, 673 (2010).
- [13] J.R. Danielson, D.H.E. Dubin, R.G. Greaves and C.M. Surko, *Rev. Mod. Phys.* **87**, 247 (2015).
- [14] J. Fajan and C.M. Surko, *Phys. Plasmas* **27**, 030601 (2020).
- [15] R. Takai, H. Enokizono, K. Ito *et al.*, *Jpn. J. Appl. Phys.* **45**, 5332 (2006).
- [16] H. Okamoto, M. Endo, K. Fukushima *et al.*, *Nucl. Instrum. Meth. A* **733**, 119 (2014).
- [17] K. Moriya, M. Ota, K. Fukushima *et al.*, *Phys. Rev. Accel. Beams* **19**, 114201 (2016).
- [18] K. Ito, H. Okamoto, Y. Tokashiki and K. Fukushima, *Phys. Rev. Accel. Beams* **20**, 064201 (2017).
- [19] J.D. Prestage, G.J. Dick and L. Maleki, *J. Appl. Phys.* **66**, 1013 (1989).
- [20] D.J. Berkland, J.D. Miller, J.C. Bergquist, W.M. Itano and D.J. Wineland, *J. Appl. Phys.* **83**, 5025 (1998).
- [21] S.A. Diddams, Th. Udem, J.C. Bergquist *et al.*, *Science* **293**, 825 (2001).
- [22] S.M. Brewer, J.-S. Chen, A.M. Hankin *et al.*, *Phys. Rev. Lett.* **123**, 033201 (2019).
- [23] E.A. Burt, J.D. Prestage, R.L. Tjoelker *et al.*, *Nature* **595**, 43 (2021).
- [24] P.K. Ghosh, *Ion Traps* (Clarendon, Oxford, 1995).
- [25] H. Okamoto, K. Kojima and K. Ito, *Prog. Theor. Exp. Phys.* **2019**, 093G01 (2019).
- [26] R.F. Bonner, J.E. Fulford, J.E. Fulford and R.E. March, *Int. J. Mass Spectrom. Ion Phys.* **24**, 255 (1977).
- [27] *Handbook of Accelerator Physics And Engineering*, edited by A.W. Chao and M. Tigner (World Scientific, Singapore, 1999), 3rd printing.
- [28] E.D. Courant and H.S. Snyder, *Ann. Phys.* **3**, 1 (1958).
- [29] K. Ito, K. Nakayama, S. Ohtsubo, H. Higaki and H. Okamoto, *Jpn. J. Appl. Phys.* **47**, 8017 (2008).
- [30] K. Ito, M. Matsuba and H. Okamoto, *Prog. Theor. Exp. Phys.* **2018**, 023G01 (2018).